Damped and delayed sinuosidal model for transient modeling

Remy Boyer, Karim Abed-Meraim

Damped and Delayed Sinusoidal Model for Transient Signals

Rémy Boyer* and Karim Abed-Meraim†

Abstract— **In this work, we present the Damped and Delayed Sinusoidal (DDS) model, a generalization of the sinusoidal model. This model takes into account an angular frequency, a damping factor, a phase, an amplitude and a time-delay parameter for each component. Two algorithms are introduced for the DDS parameter estimation using a subband processing approach. Finally, we derive the Cramer-Rao Bound (CRB) expression for the DDS model and a simulation-based performance analysis in the context of a noisy fast time-varying synthetic signal and in the audio transient signal modeling context.**

Keywords— **Transient signal, damped and delayed sinusoids, Fourier analysis, deflation, subband parameter estimation, Cramer-Rao Bound.**

I. Introduction

PARAMETRIC models such as the constant-amplitude sinusoidal or EDS (Exponentially Damped Sinusoidal) models are popular and efficient tools in many areas of interest including spectral-line [24] or pole estimation [15], source localization [22], biomedical signal processing [25] and audio signal compression [2], [12], [20]. In this paper, we introduce a generalization of these models, named the Damped and Delayed Sinusoidal (DDS) model which adds a time-delay parameter to allow time-shifting of each component waveform. Note that this paper goes further into the work initiated in [3]. Properties of this model are studied and we show that it can achieve compact representations of fast time-varying or "transient" signals.

This paper also addresses the problem of the DDS model parameter estimation. Two model parameter estimation algorithms are derived and their performances are compared on a noisy synthetic signal and on a typical audio transient signal.

The paper is organized as follows: Section II introduces the DDS model. An overview of the problems and the proposed solutions is presented in section III. In section IV, two algorithms, named DDS-B (B stands for Block), and DDS-D (D stands for Deflation), are presented for the estimation of the DDS signal parameters. Section V presents the derivation of the Cramer-Rao Bound (CRB) for the estimation of the DDS parameters in the presence of additive white Gaussian noise. Section VI provides additional comments about the DDS model and the proposed estimation algorithms. In section VII, simulation results are given and section VIII is dedicated to the final conclusions.

* University of Paris XI-Orsay and L2S-Supélec (Signals and System Lab.), Gif-Sur-Yvette, France, E-mail: remy.boyer@lss.supelec.fr.

† GET-ENST, Paris Cedex 13, France. E-mail: abed@tsi.enst.fr.

II. The DDS model

A. Parametric model definitions

The complex M-EDS model definition is given by:

$$\hat{x}(n) \stackrel{\triangle}{=} \sum_{m=1}^{M} a_m e^{i\phi_m} \cdot e^{(i\omega_m + d_m)n} \tag{1}$$

where M is the number of complex sinusoids or the modeling order and $\{a_m, \phi_m, d_m, \omega_m\}_{1\leq m\leq M}$ are the $4M$ real amplitude, phase, damping factor and angular frequency parameters. Note that if we choose $d_m = 0$ for all m, we obtain the complex sinusoidal model. The M-DDS model can be understood as a generalization of the previous parametric model. Its expression [3], [9] is given by:

$$\hat{x}(n) \stackrel{\triangle}{=} \sum_{m=1}^{M} a_m e^{i\phi_m} \cdot e^{(i\omega_m + d_m)(n-t_m)} \cdot \psi(n-t_m) \tag{2}$$

where we have introduced the discrete-valued time-delay parameters $\{t_m\}$ and the Heaviside function defined by $\psi(n) = 1$ for $n \geq 0$ and 0 otherwise. Note that the complex M-DDS model is formally similar to the M-EDS model of expression (1) by supposing that the amplitude varies with time according to:

$$\hat{x}(n) = \sum_{m=1}^{M} \tilde{a}_m(n)\ e^{i\tilde{\phi}_m} \cdot e^{(i\omega_m + d_m)n} \tag{3}$$

with $\tilde{a}_m(n) = a_m e^{-d_m t_m}\psi(n-t_m)$ and $\tilde{\phi}_m = \phi_m - t_m\omega_m$.

Real formulation of the previous complex M-DDS model can be written in terms of the complex amplitude $2\alpha_m = a_m e^{i\phi_m}$ and the pole $z_m = e^{i\omega_m + d_m}$, according to:

$$\hat{x}(n) \quad = \quad \sum_{m=1}^{M} p_m(n) \tag{4}$$

where $p_m(n) = (\alpha_m z_m^{n-t_m} + \alpha_m^* z_m^{*(n-t_m)})\psi(n-t_m)$ is a real 1-DDS component. In figure 1, different 1-DDS waveforms are presented.

B. Damping factor sign and compact representation

In this paper, we consider the real discrete space $\ell^2(\mathbb{R})$ of finite energy signals. The 1-EDS and 1-DDS signals for $d_m < 0$ belong to this space. However, sinusoidal components with $d_m > 0$ are required to model signals with strong onset when using the M-EDS model. Consequently, a large number of components $M \gg 1$ is used to mitigate

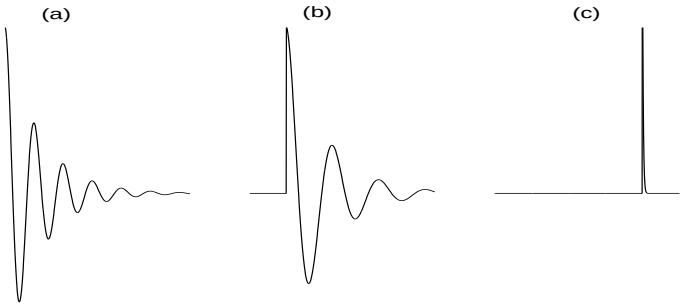

Fig. 1. 1-DDS waveforms: (a) $d_1 < 0$ and $t_1 = 0$, (b) $d_1 < 0$ and $t_1 \neq 0$, (c) $d_1 \approx -1$ (very narrow time support) and $t_1 \neq 0$

the increasing energy of such components during the analysis segment. In other words, those phenomena cannot be modeled in a compact way by a sum of 1-EDS with positive damping factor. A *compact* representation is one in which:

$$M \ll N \quad \text{and} \quad \sum_{n=0}^{N-1} |x(n) - \hat{x}(n)|^2 \ll \sum_{n=0}^{N-1} |x(n)|^2 \qquad (5)$$

where $x(n)$ is an original signal sample of length N.
On the other hand, signals with strong onset can be efficiently modeled by a sum of 1-DDS components all with negative damping factor. The strong onset is taken into account by the introduction in the model of the delay parameters $\{t_m\}$. Other approaches to handle this problem can be found in [8], [10], [16], [17], [21].

C. Time-frequency considerations

It is important to note that the 1-DDS model enables temporal representations with reduced support. This property of temporal support compactness, allows the effective modeling of any event which has fast temporal variations or which does not occupy the entire analysis segment. We note that the standard sinusoidal model does not possess this interesting property, which explains its poor performance for transient signals. The 1-EDS model is able to model signals with narrow support by imposing a large numeric value for the $|d_m|$ parameter but only at the beginning or at the end of the time analysis interval. When a signal abruptly "appears" far from the beginning of the analysis segment, the 1-EDS model is less efficient [2], [18]. The 1-DDS model with its delay parameter and with the heaviside function ($\psi(n)$) is able to model more efficiently a transient phenomenon being situated not only at the beginning or the end of the analysis segment but also in the middle of the analysis segment.

For a better understanding of these kind of transient signals, it is interesting to study their properties in the Time-Frequency (T-F) plane. In figure 2, we show simple representations of the T-F distributions of the sinusoidal, 1-EDS and 1-DDS models. The sinusoidal model uses all the time resource Δ_t and by invoking the duality principle, the frequency resource Δ_f is minimal (see figure 2-a). The 1-EDS model reduces the time resource occupation by adding a damping parameter and gets a trade-off between the time and frequency resource occupation. However, this trade-off can only be reached at the beginning and at the end of the analysis segment (see figure 2-b). The 1-DDS model with the delay parameter and the function $\psi(n)$ allows the modeling of any event occurring in the T-F plane (see figure 2-c). Contrary to the sinusoidal models and 1-EDS model, the 1-DDS model realizes a *non-forced* tiling of the T-F plane.

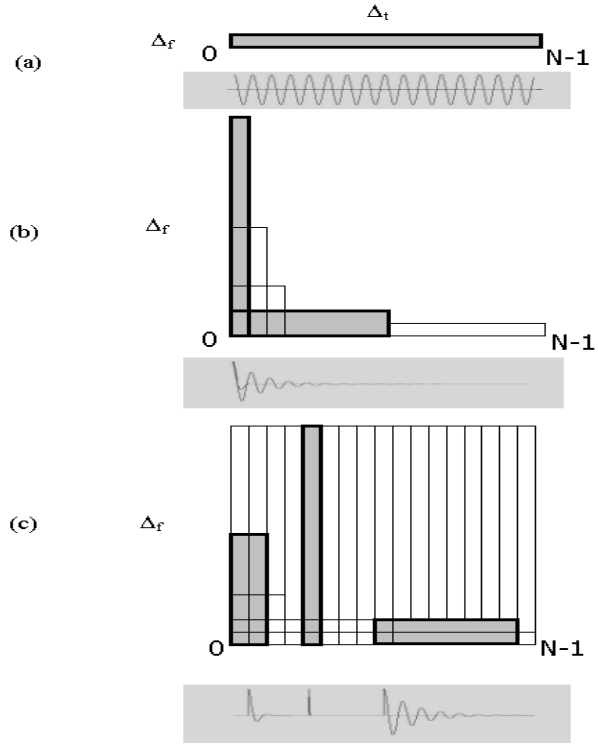

Fig. 2. Representations in the time-frequency plane (a) sinusoidal model, (b) 1-EDS model ($d \leq 0$), (c) 1-DDS model ($d \leq 0$)

III. Sketch of the solution

Given a (real-valued) signal $x(n)$, the global nonlinear criterion to be solved is:

$$\arg \min_{\{\alpha_m, z_m, t_m\}} \sum_{n=0}^{N-1} |x(n) - \hat{x}(n)|^2 \qquad (6)$$

where $\hat{x}(n)$ is the M-DDS signal given by (4).
Let $\boldsymbol{p}_m$ be the N-sample 1-DDS component, *i.e.* $\boldsymbol{p}_m = (p_m(0) \dots p_m(N-1))^T$. We can consider two cases:
• In the first case, the components are quasi-orthogonal. In other words, for $t_j \neq t_m$, we have $\langle |\boldsymbol{p}_m|, |\boldsymbol{p}_j| \rangle \approx 0$ where $\langle ., . \rangle$ defines the inner product and $|\boldsymbol{p}_m| \triangleq (|p_m(n)|)_{0 \leq n \leq N-1}$. This definition can be seen as a separation constraint on the component time-supports. Indeed, if we fix $t_m < t_j$, the component $\boldsymbol{p}_m$ has a sharp decreasing part (large damping factor) in such a way that the component $\boldsymbol{p}_j$ is practically not disrupted. This approach is studied in [4] where we propose several algorithms well adapted to the audio signals.

• In the second case, the components are non-orthogonal and $|\langle|\boldsymbol{p}_m|, |\boldsymbol{p}_j|\rangle|$ is not (approximately) equal to zero when $t_m \neq t_j$. This means that the j-th component is not clearly separated from the m-th component and direct estimation of the time delay is a difficult task. However, the angular frequency estimation by means of Fourier-type [19] or subspace [15] methods, directly applied to the observed signal, remains relatively robust while a direct damping factor estimation, on the 1-DDS signal, is systematically biased. Simulations in figure 3-a,b show these considerations on an example of a 1-DDS signal. In this context, we propose to solve this problem by performing a narrow band-pass filtering around each component to decrease the influence of the other components [27]. Afterwards, in each subband, we estimate the 1-DDS model parameters.

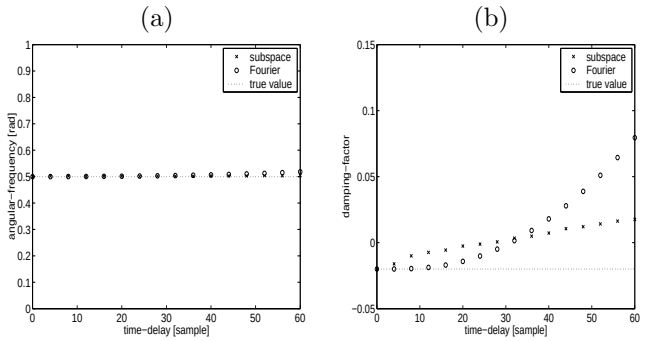

Fig. 3. 100-sample 1-DDS component (a) estimated angular frequency, (b) estimated damping factor.

In brief, the proposed parameter estimation approach proceeds in the following steps:

• Angular frequency estimation using a subspace (eventually a Fourier-type) method.

• Subband filtering to 'separate' the sinusoidal components and mitigate at best the inter-components interferences.

• In each subband, estimate the damping factor, the phase, the amplitude and the delay (eventually refine the frequency estimation) of the considered component.

Note that subband sinusoidal modeling has been already considered in [1], [7]. Contrary to our approach, the subband filtering in [1], [7] does not depend on the angular frequency of the considered signal components and is used rather to provide a perceptually improved allocation of the sinusoids.

IV. Transient modeling based on the DDS model

In [3], we have presented a new algorithm named DDS-B (B stands for Block) for the estimation of the M-DDS model parameters. This algorithm is based on the use of subspace methods and exploits a filter-bank architecture. We start by reviewing the details of this algorithm and then introduce a second estimation algorithm that uses a deflation approach in conjunction with the filter-bank architecture. The latter, named DDS-D (where D stands for deflation), is shown to improve the computational cost by using FFT-based estimation procedures.

A. DDS-B algorithm: "Block approach"

A.1 Primary estimation of the angular frequency by a subspace approach

In the context of the DDS-B algorithm, we perform a primary[1] estimation of the M angular frequency $\{\omega_m^{(1)}\}_{1\leq m\leq M}$ of the signal $x(n)$ using a standard subspace method. In this paper, we use the Matrix Pencil (MP) method [15].

Note that the MP method has been developed for the EDS but not the DDS model. In fact, the subspace shift-invariance property on which the MP method is based is only approximately satisfied in the case of DDS signals. Consequently, the corresponding parameter estimates are systematically biased. However, as observed in our simulations, the frequency parameter estimates are quite robust to this model approximation (model error) which justifies the proposed approach. This point deserves a theoretical model error perturbation analysis to evaluate the limits of this approximation and further justify our approach. This will be the focus of future work.

A.2 Filter-bank design

A filter-bank approach is considered in the DDS-B algorithm. The signal $x(n)$ is filtered as (see figure 4):

$$y_m(n) \stackrel{\triangle}{=} h_m(n) * x(n) \tag{7}$$

where $h_m(n)$ is the band-pass filter and $y_m(n)$ is the contribution of the signal in the frequency bin centered at $\omega_m^{(1)}$ ($*$ denotes the convolution operator). The design of the

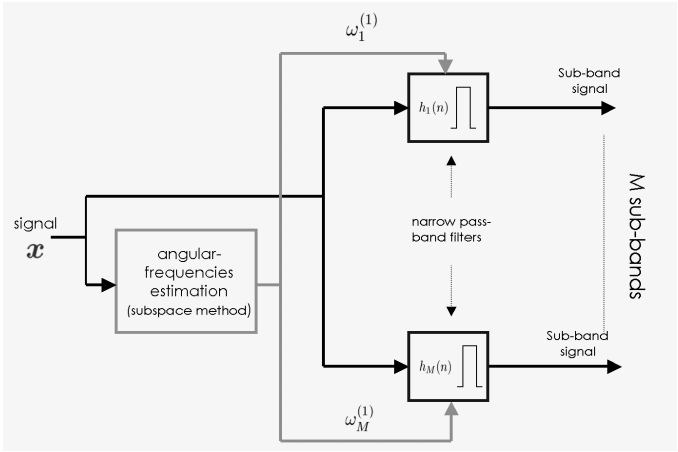

Fig. 4. Filter-bank architecture

filter $h_m(n)$ is very important since we must find a trade-off between the frequency selectivity of the filter and its time support occupation. The time-frequency uncertainty principle binds these two quantities. Indeed, filtering a transient signal without substantially degrading the time waveform implies choosing a short linear-phase FIR filter

[1]The angular frequency will be re-estimated (refined) after subband processing.

(typically between 8 and 12 coefficients). On the other hand, choosing a filter with short time support decreases, both, the frequency selectivity and the component separation ability of the filter. A good choice to balance this trade-off is the modulated raised cosine filter of length P, defined by [13]:

$$h_m(n) = \frac{\Delta}{\pi}\,\mathrm{sinc}\left(\frac{\Delta n}{2}\right)\frac{\cos\left(\varrho\frac{\Delta n}{2}\right)}{1-\varrho^2\left(\frac{\Delta n}{2}\right)^2}\,.\,\cos\left(\omega_m^{(1)}n\right) \quad (8)$$

where ϱ is the roll-off parameter and Δ is the filter bandwidth. Another possibility, when the number of components M is relatively small, would be to use a rejection filter of order $2M$ that cancels frequencies $\omega_j^{(1)}$ for $j \neq m$ and keeps only the desired one $\omega_m^{(1)}$.

A.3 Models Equivalence and filtering effects

By supposing that the m-th subband signal $y_m(n)$ is well isolated from the other components by the filtering process, we introduce the following time offset:

$$\tau_m \triangleq \arg\max_{0\leq n\leq N-1}|y_m(n)| \quad (9)$$

which represents a rough overestimate of delay parameter t_m. After that, we define the truncated subband signal:

$$\bar{y}_m(n) = y_m(n+\tau_m), \quad \text{for} \quad n = 0,\ldots,N_m-1 \quad (10)$$

with $N_m = N - \tau_m$. The latter is efficiently approximated by the real 1-EDS model. This assumption is based on the Model Equivalence (ME) property [4] between the 1-EDS model and the 1-DDS with a reduced time support and modified complex amplitude, *ie.* $\bar{y}_m(n)$ is a 1-EDS signal. Indeed, the τ_m delayed 1-DDS component can be written as:

$$\begin{aligned} p_m(n+\tau_m) &= (\alpha_m z_m^n z_m^{\tau_m - t_m} \quad (11)\\ &\qquad +\alpha_m^* z_m^{*n} z_m^{*(\tau_m - t_m)})\psi(n+\tau_m-t_m)\\ &= \alpha_m z_m^{P_m} z_m^n + \alpha_m^* z_m^{*P_m} z_m^{*n} \quad (12)\end{aligned}$$

where $P_m \triangleq \tau_m - t_m$.
Using the fact that $p_m(n)$ is causal, *ie.*, $\psi(n+a) = \psi(n)$ for $n \geq 0$ and $a \geq 0$, we verify that expression (11) is the 1-EDS model definition with modified complex amplitude. Using the previous ME property, the estimate of the truncated subband signal admits the following expression:

$$\begin{aligned}\hat{\bar{y}}_m(n) &= \sum_{k=0}^{P_m-1} h_m(k)p_m(n-k+\tau_m)\\ &= \alpha_m H(z_m) z_m^n + \alpha_m^* H(z_m^*) z_m^{*n}\\ &= \tilde{\alpha}_m z_m^n + \tilde{\alpha}_m^* z_m^{*n} \quad (13)\end{aligned}$$

with $H(z) = z^{P_m}\sum_{k=0}^{P_m-1} h_m(k)z^{-k}$ (due to the filtering properties, we have $P_m = P$ where P is the time-delay introduced by the filter). Consequently, we can see that only the complex amplitude is modified by the filter $h_m(n)$ according to:

$$\tilde{\boldsymbol{\alpha}}_m \triangleq \boldsymbol{S}_m\boldsymbol{\alpha}_m \text{ where } \boldsymbol{S}_m = \mathrm{diag}\{H(z_m), H(z_m^*)\} \quad (14)$$

with $\tilde{\boldsymbol{\alpha}}_m \triangleq (\tilde{\alpha}_m\ \tilde{\alpha}_m^*)^T$ and $\boldsymbol{\alpha}_m \triangleq (\alpha_m\ \alpha_m^*)^T$ is the complex amplitude vector.

A.4 Subband parameter estimation

In each subband indexed by m, we estimate the filtered 1-DDS component $\hat{y}_m(n) \triangleq h_m(n) * p_m(n)$ which best matches the m-th filtered signal $y_m(n)$ (see figure 5), *ie.*, we resolve the following criterion:

$$\arg\min_{\boldsymbol{\alpha}_m,\boldsymbol{z}_m,t_m}\varepsilon_m \quad (15)$$

where:

$$\varepsilon_m \triangleq \sum_{n=0}^{N-1}|y_m(n)-\hat{y}_m(n)|^2 = ||\boldsymbol{y}_m - \boldsymbol{H}_m\boldsymbol{G}(\boldsymbol{z}_m,t_m)\boldsymbol{\alpha}_m||^2 \quad (16)$$

where $\boldsymbol{H}_m$ is the $N\times N$ filtering matrix, given by:

$$\boldsymbol{H}_m = \begin{pmatrix} h_m(0) & 0 & \ldots & \ldots & 0\\ \vdots & \ddots & \ddots & & \vdots\\ h_m(P-1) & & \ddots & \ddots & \vdots\\ \vdots & \ddots & & \ddots & 0\\ 0 & \ldots & h_m(P-1) & \ldots & h_m(0)\end{pmatrix}. \quad (17)$$

$\boldsymbol{y}_m$ is the N-sample subband signal, $\boldsymbol{z}_m = (z_m\ z_m^*)^T$ is the pole vector and $\boldsymbol{G}(\boldsymbol{z}_m,t_m)$ is the $N\times 2$ zero-padded Vandermonde matrix defined by:

$$\boldsymbol{G}(\boldsymbol{z}_m,t_m) \triangleq \begin{pmatrix} \boldsymbol{0}_{t_m} & \boldsymbol{0}_{t_m}\\ 1 & 1\\ z_m & z_m^*\\ \vdots & \vdots\\ z_m^{N-t_m-1} & z_m^{*(N-t_m-1)}\end{pmatrix}. \quad (18)$$

Assuming an initial estimate of the time-delay, criterion (15) is equivalent to the following one:

$$\arg\min_{\boldsymbol{\alpha}_m,\boldsymbol{z}_m}||\bar{\boldsymbol{y}}_m - \boldsymbol{J}_m\boldsymbol{G}(\boldsymbol{z}_m,\tau_m)\boldsymbol{S}_m\boldsymbol{\alpha}_m||^2 \quad (19)$$

where $\boldsymbol{J}_m$ is a $N_m\times N$ selection matrix such as $\bar{\boldsymbol{y}}_m = \boldsymbol{J}_m\boldsymbol{y}_m$.

Angular frequency and damping factor estimation: The direct minimization of criterion (15) or (19) requires a computationally expensive multidimensional nonlinear optimization. Instead, we propose a much simpler approach based on the signal FFT where angular frequency is re-estimated (this is a refining of the first estimate $\omega_m^{(1)}$) according to:

$$\omega_m^{(2)} = \arg\max_{\lambda\in[0,\pi[}|\bar{Y}_m(\lambda)| \quad (20)$$

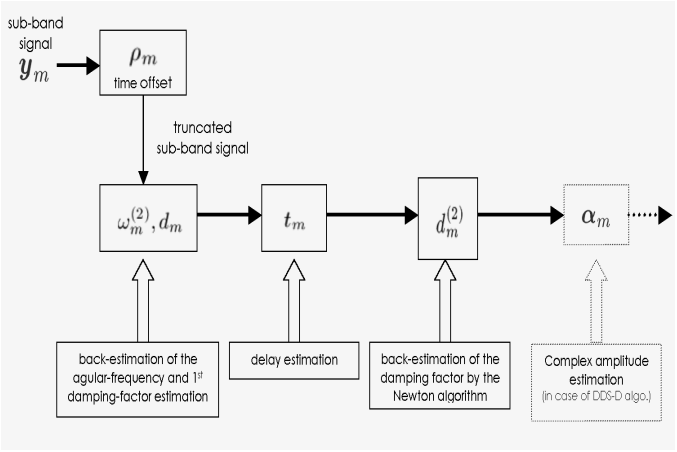

Fig. 5. Subband signal processing

where $\bar{Y}_m(\lambda)$ is the Fourier Transform (FT) of the truncated subband signal. After that, we estimate the damping factor $d_m^{(1)}$ by the shifted-FT method [19]. This method uses the ratio of the modulus of two FT segments of the same length but one shifted from the other. Consequently, we have:

$$d_m^{(1)} = \frac{1}{K} \ln \frac{\left|\bar{Y}_m^{(1)}(\omega_m^{(2)})\right|}{\left|\bar{Y}_m^{(0)}(\omega_m^{(2)})\right|} \tag{21}$$

where $\bar{Y}_m^{(0)}(\lambda)$ and $\bar{Y}_m^{(1)}(\lambda)$ are the respective FTs of the signals:

$$\begin{array}{lcll} \bar{y}_m^{(0)}(n) & \triangleq & \bar{y}_m(n)w(n) & \text{for} \quad n = 0, \ldots, N_m - K - 1 \\ \bar{y}_m^{(1)}(n) & \triangleq & \bar{y}_m(n)w(n-K) & \text{for} \quad n = K, \ldots, N_m - 1 \end{array}$$

where K is a time offset chosen to be small with respect to the analysis duration. $w(n)$ is a smooth window which is designed for isolating the pole from its conjugate. We choose here a Blackman window.

Time delay estimation: The delay parameter is estimated via a 'model-data' matching criterion. Therefore, in each subband m, we resolve criterion (15) with respect to the time-delay. Given an estimate of the complex pole $\hat{z}_m \triangleq e^{i\omega_m^{(2)}+d_m^{(1)}}$ and optimizing first over the amplitude and then over t leads to:

$$t_m = \arg \min_{t \in \mathcal{V}(\tau_m)} f(d_m^{(1)}, t) \text{ where } f(d,t) \triangleq ||\boldsymbol{\Pi}_{\mathcal{G}}^{\perp}(d,t)\boldsymbol{y}_m||^2 \tag{22}$$

where $\boldsymbol{\Pi}_{\mathcal{G}}^{\perp}(d,t) = \boldsymbol{I}_N - \boldsymbol{\mathcal{G}}\boldsymbol{\mathcal{G}}^{\dagger}$ is the orthogonal projector onto the kernel of $\boldsymbol{\mathcal{G}}(\hat{\boldsymbol{z}}_m, t) \triangleq \boldsymbol{H}_m \boldsymbol{G}(\hat{\boldsymbol{z}}_m, t)$ the filtered matrix of the m-th signal pole. $\boldsymbol{\mathcal{G}}^{\dagger}$ is the pseudo-inverse of $\boldsymbol{\mathcal{G}}$ and $\mathcal{V}(\tau_m)$ is a given time interval centered at $\tau_m - P$. We solve (22) by a simple enumeration of the possible values in $\mathcal{V}(\tau_m)$, so as to reduce the search cost.

Back-estimation of the damping factor: Once we estimate the delay t_m we can sharpen the damping factor estimation using a nonlinear optimization technique such as Newton's algorithm [5]. The back-estimation (using Newton's method) of the damping factor corresponds to:

$$d_m^{(2)} = d_m^{(1)} - \left(\frac{\partial^2 f}{\partial d^2}(d_m^{(1)}, t_m)\right)^{-1} \frac{\partial f}{\partial d}(d_m^{(1)}, t_m), \tag{23}$$

which can be iterated to further improve the estimation of the damping parameter.
We give the expressions of the first and the second order derivative with respect to the damping factor as:

$$\begin{aligned} \frac{\partial f}{\partial d}(d, t_m) &= 2\Re e\{\boldsymbol{y}_m^T \boldsymbol{\Pi}_{\mathcal{G}}^{\perp} \boldsymbol{\mathcal{G}}' \boldsymbol{\mathcal{G}}^{\dagger} \boldsymbol{y}_m\} \\ \frac{\partial^2 f}{\partial d^2}(d, t_m) &= 2\Re e\{\boldsymbol{y}_m^T (\boldsymbol{\Pi}_{\mathcal{G}}^{\perp}(\boldsymbol{\mathcal{G}}''\boldsymbol{\mathcal{G}}^{\dagger} + \boldsymbol{\mathcal{G}}'\boldsymbol{\mathcal{G}}^{\dagger\prime}) \\ &\quad -(\boldsymbol{\mathcal{G}}'\boldsymbol{\mathcal{G}}^{\dagger} + \boldsymbol{\mathcal{G}}\boldsymbol{\mathcal{G}}^{\dagger\prime})\boldsymbol{\mathcal{G}}'\boldsymbol{\mathcal{G}}^{\dagger})\boldsymbol{y}_m\} \end{aligned} \tag{24}$$

where $\boldsymbol{\mathcal{G}}^{\dagger\prime} = (\boldsymbol{\mathcal{G}}^H\boldsymbol{\mathcal{G}})^{-1}(\boldsymbol{\mathcal{G}}^{H\prime} - (\boldsymbol{\mathcal{G}}^{H\prime}\boldsymbol{\mathcal{G}} + \boldsymbol{\mathcal{G}}^H\boldsymbol{\mathcal{G}}')(\boldsymbol{\mathcal{G}}^H\boldsymbol{\mathcal{G}})^{-1})$ and $\boldsymbol{\mathcal{G}}'$ (respectively $\boldsymbol{\mathcal{G}}''$) denotes the first (respectively second) order derivative of $\boldsymbol{\mathcal{G}}$ with respect to the parameter d.
In order to simplify the above re-estimation procedure, we use in our simulation a Newton implementation based on the real-valued (instead of complex) vectors which lead to vector instead of matrix manipulations according to:

$$d_m^{(2)} = d_m^{(1)} - \frac{\tilde{f}'(d_m^{(1)})}{\tilde{f}''(d_m^{(1)})} \tag{25}$$

where $\tilde{f}(d) \triangleq (\boldsymbol{\mathcal{G}}_d^T \boldsymbol{y}_m)^2$ with $\boldsymbol{\mathcal{G}}_d = (\mathcal{G}_d(0), \cdots, \mathcal{G}_d(N-1))^T$ and:

$$\mathcal{G}_d(n) \triangleq e^{d(n-t_m)} \cos(\omega_m^{(2)}(n-t_m) + \hat{\phi}_m)\psi(n-t_m). \tag{26}$$

where $\hat{\phi}_m$ represents an estimate of the phase parameter given by $2\hat{\phi}_m = \angle\alpha_m(1) - \angle\alpha_m(2)$ where $\boldsymbol{\alpha}_m = (\alpha_m(1)\ \alpha_m(2))^T$ is estimated as shown in subsection B.2 using $\hat{z}_m$ and $\angle$ denotes the phase argument.

A.5 Complex amplitude estimation

In the context of DDS-B algorithm, we proceed to the amplitude and phase parameter estimation according to the linear least squares criterion:

$$\min_{\boldsymbol{\alpha}} \|\boldsymbol{x} - \boldsymbol{G}(\hat{\boldsymbol{z}}, \boldsymbol{t})\boldsymbol{\alpha}\|^2 \tag{27}$$

where $\boldsymbol{x} = (x(0) \ldots x(N-1))^T$ is the observed signal vector and:

$$\boldsymbol{G}(\hat{\boldsymbol{z}}, \boldsymbol{t}) = \begin{bmatrix} \boldsymbol{G}(\hat{\boldsymbol{z}}_1, t_1) & \boldsymbol{G}(\hat{\boldsymbol{z}}_2, t_2) & \ldots \boldsymbol{G}(\hat{\boldsymbol{z}}_M, t_M) \end{bmatrix} \tag{28}$$

is a block-Vandermonde matrix with $\hat{z}_m \triangleq e^{i\omega_m^{(2)}+d_m^{(2)}}$ and $\boldsymbol{\alpha} = (\boldsymbol{\alpha}_1^T \ldots \boldsymbol{\alpha}_M^T)^T$. We finally extract the M real amplitudes $\{a_m\}$ and the M phases $\{\phi_m\}$ from:

$$\boldsymbol{\alpha} = \boldsymbol{G}(\hat{\boldsymbol{z}}, \boldsymbol{t})^{\dagger} \boldsymbol{x} \tag{29}$$

according to $2a_m = |\alpha_m(1)| + |\alpha_m(2)|$ and $2\phi_m = \angle\alpha_m(1) - \angle\alpha_m(2)$. Note that, if needed, it is possible to use a real formulation [3] to reduce the computational complexity.

B. DDS-D algorithm: "Deflation approach"

We propose here a second algorithm which is based on a Fourier-type iterative scheme with deflation to enforce the 1-DDS separation. This approach presents a lower computational complexity than the DDS-B approach. Such iterative schemes are very efficient and have been considered in the literature in many signal processing problems and in particular in the context of the Matching-Pursuit technique [11], [14].

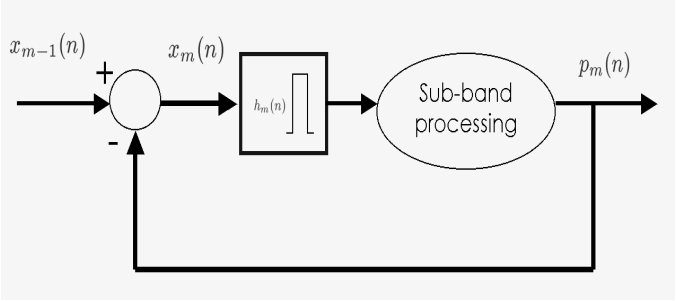

Fig. 6. "Deflation" architecture

Consider the m-th residual signal defined by the recurrent equation:

$$x_m(n) \triangleq x_{m-1}(n) - p_m(n) = x(n) - \sum_{j=1}^{m} p_j(n) \qquad (30)$$

where $x_0(n) = x(n)$. Contrary to the DDS-B algorithm, we determine a primary angular frequency $\omega_m^{(1)}$ estimation by simply maximizing the FT modulus of the m-th residual signal according to $\omega_m^{(1)} = \max_{\omega\in[0,\pi]} |X_m(\omega)|$ where $X_m(\omega)$ is the FT of the signal $x_m(n)$. Note that for the deflation process, the signal $p_j(n)$ in expression (30) should be known, which means that its corresponding amplitude, phase and damping factor have been estimated. This is detailed in the next two following sections.

We denote the m-th synthetic signal by $\hat{x}_m(n) \triangleq \sum_{j=1}^{m} p_j(n)$ and from expression (30), we have:

$$\tilde{\varepsilon}_m \triangleq \sum_{n=0}^{N-1} |x_m(n)|^2 = \sum_{n=0}^{N-1} |x(n) - \hat{x}_m(n)|^2. \qquad (31)$$

This process is stopped when the energy of the residual is small enough, according to $\tilde{\varepsilon}_m \leq \epsilon . \sum_{n=0}^{N-1} |x(n)|^2$ where $\epsilon > 0$ is a chosen threshold.

For estimating the sinusoid parameters, we use the above deflation technique in conjunction with subband filtering to enforce the separation of the different components. In this algorithm, we applied the modulated raised cosine filter, defined in section IV-A.2, but in the context of DDS-D algorithm, *ie.* it is the m-th residual signal which is filtered such as:

$$y_m(n) \triangleq h_m(n) * x_m(n). \qquad (32)$$

After that, we perform the angular frequency back-estimation and damping factor estimation according to the methodology of section IV-A.4 and the time-delay estimation and damping factor back-estimation as described in previous sections.

Moreover, we have to estimate the complex amplitude (amplitude and phase parameter) of the subband signal according to the linear least squares criterion (19). Define $\hat{z}_m \triangleq e^{d_m^{(2)} + i\omega_m^{(2)}}$. We extract the real amplitude a_m and the phase ϕ_m in terms of the complex amplitude associated to the m-th subband signal:

$$\boldsymbol{\alpha}_m = \boldsymbol{S}_m^{-1} \left(\boldsymbol{J}_m \boldsymbol{G}(\hat{\boldsymbol{z}}_m, \tau_m)\right)^{\dagger} \bar{\boldsymbol{y}}_m. \qquad (33)$$

V. Cramer-Rao Bound for the DDS model

The CRB for the parameter estimation of a DDS process is derived in this section since it is useful as a touchstone against which the efficiency of the considered estimators can be tested. The CRB has been investigated in [23] for an undamped sinusoidal process and in [28] for a damped sinusoidal process. We derive, here, the conditional CRB for the more general DDS case. More precisely, the CRB is computed conditionally to the exact knowledge of the discrete-valued time-delay parameters.

Consider a real-valued M-DDS process corrupted by zero-mean white gaussian noise $e(n)$:

$$x(n) = \hat{x}(n) + e(n), \quad n = 0, \ldots, N-1 \qquad (34)$$

where $\hat{x}(n)$ is given by (4). Let $\boldsymbol{\gamma} = [\boldsymbol{d}^T, \boldsymbol{\omega}^T, \boldsymbol{\phi}^T, \boldsymbol{a}^T]^T$ be the vector of desired damping factor, angular frequency, phase and amplitude parameters where $\boldsymbol{d} = (d_1, \ldots, d_M)^T$ and $\boldsymbol{\omega}, \boldsymbol{\phi}$ and $\boldsymbol{a}$ are defined similarly. The time-delay parameter vector $\boldsymbol{t} = (t_1, \ldots, t_M)^T$ is omitted here as it is assumed perfectly known (see discussion in section VI). Under the above assumptions, the logarithmic likelihood function can be expressed as:

$$\mathcal{L}_t(\boldsymbol{x}|\boldsymbol{\gamma}, \sigma^2) = -\frac{N}{2}\log(2\pi) - N\log\sigma^2 - \frac{\|\boldsymbol{x} - \hat{\boldsymbol{x}}\|^2}{2\sigma^2} \qquad (35)$$

where σ^2 denotes the noise power. The CRB's of the corresponding parameter estimators are given by the diagonal elements of the inverse of the Fisher Information matrix:

$$[\boldsymbol{\mathcal{F}}_t(\boldsymbol{\Theta})]_{i,j} \triangleq E\left[\frac{\partial \mathcal{L}_t(\boldsymbol{x}|\boldsymbol{\Theta})}{\partial \Theta_i} \cdot \frac{\partial \mathcal{L}_t(\boldsymbol{x}|\boldsymbol{\Theta})}{\partial \Theta_j}\right] \qquad (36)$$

with $\boldsymbol{\Theta} = [\boldsymbol{\gamma}^T, \sigma^2]^T$. Before proceeding, we first show that the CRB for $\boldsymbol{\gamma}$ is decoupled from the CRB for σ^2.

Lemma: *Under the above assumptions, the elements of the Fisher Information matrix $\boldsymbol{\mathcal{F}}_t(\boldsymbol{\gamma}, \sigma^2)$ corresponding to the cross terms of γ_k and σ^2 are zero.*

The proof of this lemma is given in the appendix. This lemma allows us to "ignore" the noise parameter and compute only the Fisher Information sub-matrix corresponding to the desired parameters $\boldsymbol{\gamma}$.

Corollary: *The CRB for the variance of any unbiased estimate of $\boldsymbol{\gamma}$ (conditionally to the perfect knowledge of the time-delay parameter vector $\boldsymbol{t}$) is given by:*

$$[\mathrm{CRB}_t(\boldsymbol{\gamma})]_{i,j} = \sigma^2 \left[\frac{\partial \hat{\boldsymbol{x}}^T}{\partial \gamma_i} \cdot \frac{\partial \hat{\boldsymbol{x}}}{\partial \gamma_j}\right]^{-1} \qquad (37)$$

where $\frac{\partial \hat{\boldsymbol{x}}}{\partial \gamma_i} \triangleq \left(\frac{\partial \hat{x}(0)}{\partial \gamma_i} \; \frac{\partial \hat{x}(1)}{\partial \gamma_i} \ldots \frac{\partial \hat{x}(N-1)}{\partial \gamma_i} \right)^T$ is given by:

$$\frac{\partial \hat{x}(n)}{\partial a_i} = e^{d_i(n-t_i)} \cos\left(\omega_i(n-t_i)+\phi_i\right)\psi(n-t_i)$$
$$\frac{\partial \hat{x}(n)}{\partial d_i} = a_i(n-t_i)e^{d_i(n-t_i)} \cos\left(\omega_i(n-t_i)+\phi_i\right)\psi(n-t_i)$$
$$\frac{\partial \hat{x}(n)}{\partial \omega_i} = -a_i(n-t_i)e^{d_i(n-t_i)} \sin\left(\omega_i(n-t_i)+\phi_i\right)\psi(n-t_i)$$
$$\frac{\partial \hat{x}(n)}{\partial \phi_i} = -a_i e^{d_i(n-t_i)} \sin\left(\omega_i(n-t_i)+\phi_i\right)\psi(n-t_i)$$

VI. Discussion

We provide here some comments to get more insight onto the proposed DDS model and related parameter estimation algorithms and CRB.

- The numerical cost of the DDS-B is essentially equal to the subspace decomposition cost plus the subband filtering cost plus the least-square resolution of equation (28). This leads to a total complexity of $O(N^3 + MN\log N + NM^2)$. On the other hand, the complexity of the DDS-D is essentially dominated by the subband filtering cost and Fourier transforms for angular frequency and damping factor estimation. Therefore, the total complexity of DDS-D is of $O(MN\log N)$ only. Note that, in both cases, the cost of the Newton algorithm is $O(NM)$ which is negligible in comparison with others implementation costs.
- In section V, we did chose to compute a bound conditionally to the exact knowledge of delay parameters because the latter are discrete-valued and consequently the computation of a (non-conditional) bound leads to intractable derivations. On the other hand, choosing time-delay parameters with continuous real valued leads to the following model indeterminacy: for $n = 0, \ldots, N-1$, we have:

$$ae^{d(n-t)}\cos(\omega(n-t)+\phi)\psi(n-t) = ae^{d(n-(t+\tau))}\cos(\omega(n-(t+\tau))+\phi+\tau\omega)\psi(n-(t+\tau))$$

for any τ such that $\lceil t+\tau \rceil = \lceil t \rceil$ where $\lceil . \rceil$ is the integer part.

- We observed in our simulation a relatively small distance (especially when the damping factor is low) between our estimation method performances and the CRB for low and moderate values of the SNR. However, the gap becomes significant for high SNRs (typically over 20 dB). This is due to the fact that at high SNRs, the performances are essentially bounded by the approximation errors of our estimation method. Indeed, we assume implicitly that the rejection filter is perfect and hence in each subband only one sinusoidal component persists. Due to the angular frequency estimation errors and the finite duration of the rejection filter, this assumption is only approximatively satisfied.
- The DDS model might be slightly modified in such a way to allow a continuous variation of the delay parameters. This can be done for example by using a *soft* DDS model where the Heaviside function used in the signal modeling is replaced by an appropriate continuous function that decreases smoothly to zero (contrary to the Heaviside function that is discontinuous at zero). This model has the particular advantage to allow exact computation of the CRB in terms of all DDS parameters including the time-delays. This point is still under investigation and will be the focus of future work.
- We can notice a certain analogy between the component cancellation schemes used in DDS-B and DDS-D algorithms and the PIC (Parallel Interference Cancellation) and SIC (Sequential Interference Cancellation) schemes used in CDMA (Code Division Multiple Access) communication systems [6], [26]. Several studies of the PIC and SIC exist in the literature and some of them can be adapted to our context. In particular, we can use a multi-stage cancellation procedure to improve the DDS parameter estimation.

VII. Simulations

A. Synthetic signal

We choose a 2-DDS non-orthogonal components, *ie.*, $|t_2 - t_1|$ is small. In this case, a time-delay estimation/detection based on the variation of the signal envelope is inefficient. We show in figure 7-a and b the test signal and the two components.

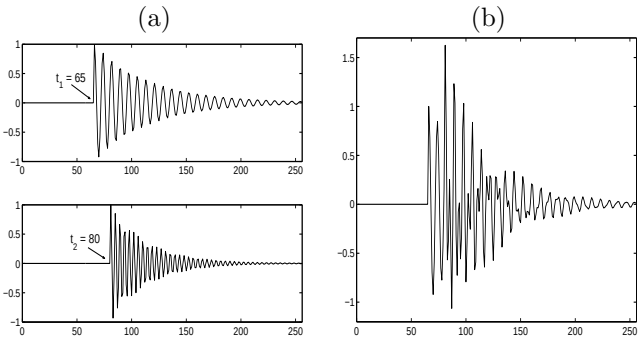

Fig. 7. (a), (top) first 1-DDS, (bottom), second 1-DDS, (b) sum of the two components

A.1 Parameter estimation analysis

The algorithms are compared in terms of parameter estimation accuracy through the Normalized Mean Square Error (NMSE), evaluated for several Signal to Noise Ratios (SNR) using 100 Monte-Carlo trials. The NMSE is defined by the ratio of the square difference between the true parameter value and its estimated value over the square value of the true parameter. Additionally, we define $\mathrm{SNR}(\hat{\boldsymbol{x}}, \sigma\boldsymbol{w}) = 10\log_{10}(||\hat{\boldsymbol{x}}||^2/\sigma^2)$. In relation to figures 8 and 9, we can say that the DDS-B algorithm outperforms the DDS-D algorithm in this simulation context for the damping factor estimation. In figure 10, we have represented the time-delay estimation for each experiment ($50 \times 8 = 400$). So every 50 experiments, we increase the SNR by 5 dB. Note that the true time-delay values are 65 and 80 and we can point out the capacity of the proposed algorithms to correctly estimate these parameters,

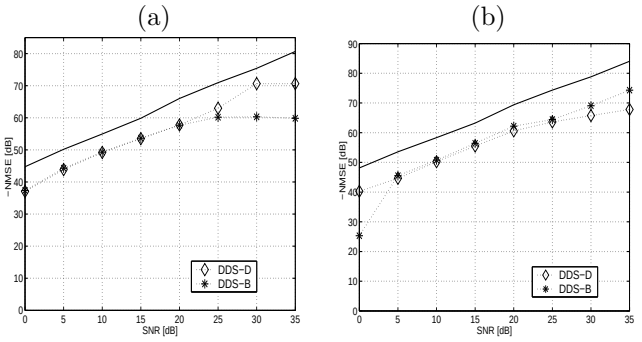

Fig. 8. Angular frequency estimation performance, (a) first component ($m = 1$), (b) second component ($m = 2$). The solid line curve corresponds to the angular frequency CRB.

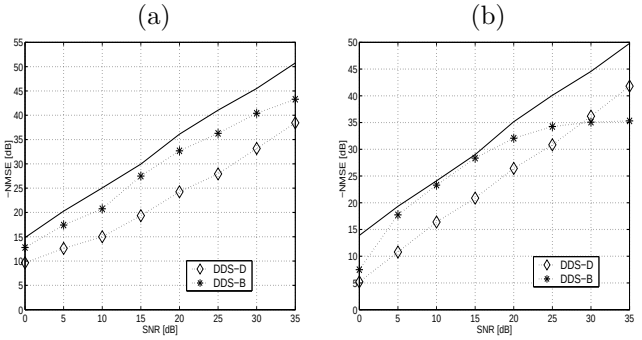

Fig. 9. Damping factors estimation performance, (a) first component ($m = 1$), (b) second component ($m = 2$). The solid line curve corresponds to the damping factor CRB.

especially at SNR higher than 15 dB. Finally, we can note that the performances of these two algorithms are quite far from the ideal performances of the CRB. We can improve the efficiency of these algorithms by considering a joint Newton algorithm in ω, d, ϕ which can be done at a slight increase of the computational complexity. This improvement has been observed for the synthetic data of figure 7. However, for percussive audio signals of the next section, the observed performance gain due to joint Newton algorithm is negligible. Consequently, we have kept a simple Newton on the parameter d only since this approach represents a good trade-off between computational complexity and performance.

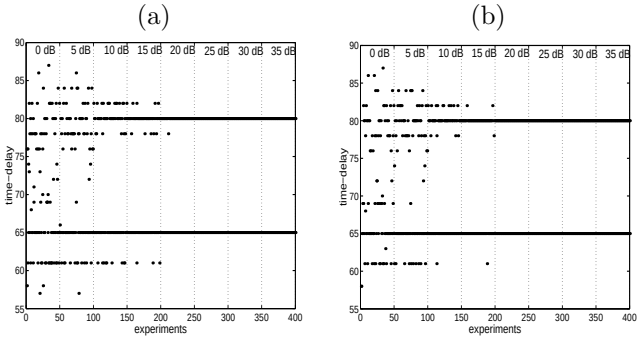

Fig. 10. Time-delays estimation for each experiment (400) (true values: 65 and 80), (a) DDS-B, (b) DDS-D

B. Typical audio transient signal

In the context of percussive audio modeling, we choose to apply the proposed algorithms on a castanet onset which is a typical audio transient signal (see the top of figure 11-a). In the middle and bottom plots, we show 20-order DDS-B and DDS-D models, respectively. The chosen criterion is the SMNR (Signal to Modeling Noise Ratio) which is a time matching criterion between the synthesized waveform and the original signal. Note that the SMNR in the context of audio modeling is defined according to $\mathrm{SMNR}(\boldsymbol{x}, \boldsymbol{r}) = 10\log_{10}(||\boldsymbol{x}||^2/||\boldsymbol{r}||^2)$ in dB where $\boldsymbol{r} = \boldsymbol{x} - \hat{\boldsymbol{x}}$ is the residual audio signal. Then, we obtain 11.2 dB for the DDS-B algorithm and 12.7 dB for the DDS-D algorithm. This result is confirmed by the observation of figure 11-b. Indeed, we can see that the DDS-B algorithm estimates several time-delay parameters lower than 223 samples which is the true onset in the original signal as indicated in figure 11-a. Consequently, we observe in figure 11-a (middle), a small pre-echo (distortion before the sound onset [2], [8]). Inversely, the DDS-D modeling presents a total absence of pre-echo and a good reproduction of the onset dynamic.

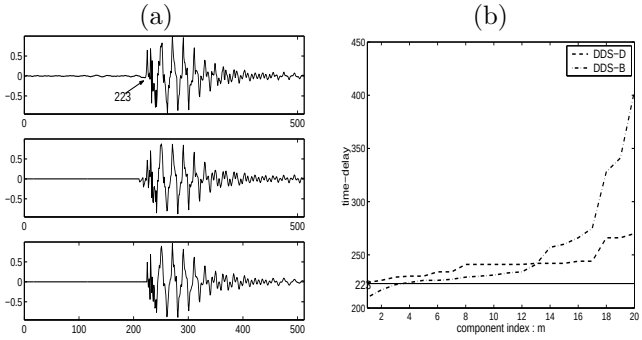

Fig. 11. (a), (top) original castanet onset (normalized amplitude), (middle) 20-order modeling by the DDS-B algorithm, (bottom) 20-order modeling by the DDS-D algorithm,(b) time-delay estimation with respect to the index component.

VIII. Conclusion

In this article, we presented a non-stationary parametric Damped and Delayed Sinusoidal (DDS) model. This model can be seen as a generalized sinusoidal model in the sense that we add damping factors and delay parameters. These modifications enable efficient modeling of any event in the time-frequency plane. We present two model parameter estimation algorithms applied to a noisy fast time-varying synthetic signal and to a typical audio transient signal. The first algorithm, named DDS-B, is based on a subspace approach and the exploitation of the use of a filter-bank scheme. The second algorithm, named DDS-D, uses a Fourier-type algorithm in conjunction with a deflation scheme. Afterwards, we estimate and back-estimate the model parameters in each subband. Finally, we derive the expression of the Cramer-Rao Bound for the DDS

model. A performance analysis shows the usefulness and validity of the proposed approach.

Appendix

Proof of the Lemma

We prove here that:

$$\forall\ i,\ E\left[\frac{\partial \mathcal{L}_t(\boldsymbol{x}|\boldsymbol{\gamma},\sigma^2)}{\partial \gamma_i}\ .\ \frac{\partial \mathcal{L}_t(\boldsymbol{x}|\boldsymbol{\gamma},\sigma^2)}{\partial \sigma^2}\right]=0.$$

For that, consider the equality:

$$E\left[\frac{\partial \mathcal{L}_t(\boldsymbol{x}|\boldsymbol{\gamma},\sigma^2)}{\partial \gamma_i}\ .\ \frac{\partial \mathcal{L}_t(\boldsymbol{x}|\boldsymbol{\gamma},\sigma^2)}{\partial \sigma^2}\right]=-E\left[\frac{\partial^2 \mathcal{L}_t(\boldsymbol{x}|\boldsymbol{\gamma},\sigma^2)}{\partial \gamma_i\ .\ \partial \sigma^2}\right].$$

where:

$$\frac{\partial^2 \mathcal{L}_t(\boldsymbol{x}|\boldsymbol{\gamma},\sigma^2)}{\partial \gamma_i\ .\ \partial \sigma^2}=\frac{1}{\sigma^4}(\boldsymbol{x}-\hat{\boldsymbol{x}})^T\frac{\partial \hat{\boldsymbol{x}}}{\partial \gamma_i}=\frac{1}{\sigma^4}\ \boldsymbol{e}^T\frac{\partial \hat{\boldsymbol{x}}}{\partial \gamma_i}$$

where $\boldsymbol{e}=(e(0)\dots e(N-1))^T$ denotes the noise vector. The latter being of zero mean, we have:

$$E\left[\frac{\partial^2 \mathcal{L}_t(\boldsymbol{x}|\boldsymbol{\gamma},\sigma^2)}{\partial \gamma_i\ .\ \partial \sigma^2}\right]=\frac{1}{\sigma^4}\ \frac{\partial \hat{\boldsymbol{x}}^T}{\partial \gamma_i}\ E[\boldsymbol{e}]=0\quad\square$$

References

[1] D. Anderson, "Speech analysis and coding using multiresolution sinusoidal transform", *Proc. of Int. Conf. on Acoustic, Speech and Signal Processing (ICASSP)*, 1996.

[2] R. Boyer, S. Essid and Nicolas Moreau, "Dynamic temporal segmentation in parametric non-stationary modeling for percussive musical signals", *IEEE Int. Conf. on Multimedia and Expo (ICME)*, 2002.

[3] R. Boyer and K. Abed-Meraim, "Audio transients modeling by Damped & Delayed Sinusoids (DDS)", *Proc. of IEEE Int. Conf. on Acoustic, Speech and Signal Processing (ICASSP)*, 2002.

[4] R. Boyer and K. Abed-Meraim, "Audio Modeling based on Delayed Sinusoids", *IEEE Trans on Speech and Audio Processing*, Vol. 12, No. 2, March 2004.

[5] J.E. Dennis, J.R. and R.B. Schnabel, *Numerical methods for unconstrained optimization and nonlinear equations*, Prentice-Hall, 1983.

[6] P.W. Dent, "CDMA subtractive demodulation", U.S. Patent 5,218,619, June 1993.

[7] T. Ellis, P.W. Daniel and B.L. Vercoe, "A wavelet-based sinusoid model of sound for auditory signal separation", *Proc. of Int. Computer Music Conference (ICMC)*, 1991.

[8] R. Gribonval, E. Bacry and S. Mallat, "Analysis of sound signals with high resolution matching pursuit", *Proc. of Time-Frequency Time-Scale Symposium*, 1996.

[9] M. Goodwin, "Matching pursuit with damped sinusoids", *Proc. of IEEE Int. Conf. on Acoustic, Speech and Signal Processing (ICASSP)*, 1997.

[10] M. Goodwin, *Adaptive Signal Models*, Kluwer, 1998.

[11] M. Goodwin, "Multiscale overlap-add sinusoidal modeling using matching pursuits and refinements", *Proc. of Workshop on Application of Signal Processing to Audio and Acoustics (WASPAA)*, 2001.

[12] K.N. Hamdy, M. Ali and A.H. Tewfik, "Low bit rate high quality audio coding with combined harmonic and wavelet representations", *Proc. of IEEE Int. Conf. on Acoustic, Speech and Signal Processing (ICASSP)*, 1996.

[13] R. Hamming, *Digital Filters*, 3rd Ed., Prentice Hall, 1989.

[14] R. Heusdens, R. Vafin and B. Kleijn, "Sinusoidal modeling of audio and speech using psychoacoustic-adaptive matching pursuit", *Proc. of IEEE Int. Conf. on Acoustic, Speech and Signal Processing (ICASSP)*, 2001.

[15] Y. Hua and T.K. Sarkar, "Matrix pencil method for estimating parameters of exponentially damped/undamped sinusoids in noise", *IEEE Trans. on Acoustic, Speech and Signal Processing*, Vol. 38, No. 5 , May 1990.

[16] S. Levine, T. Verma and J.O. Smith, "Alias-free, multiresolution sinusoidal modeling for polyphonic wideband audio", *Proc. of Workshop on Application of Signal Processing to Audio and Acoustics (WASPAA)*, 1997.

[17] S. Levine, T. Verma and J.O. Smith, "Multiresolution sinusoidal modeling forwideband audio with modifications", *Proc. of IEEE Int. Conf. on Acoustic, Speech and Signal Processing (ICASSP)*, 1998.

[18] J. Nieuwenhuijse, R. Heusdens and E.F. Deprettere, "Robust exponential modeling of audio signal", *Proc. of Int. Conf. on Acoustic, Speech and Signal Processing (ICASSP)*, 1998.

[19] P. O'Shea, "The Use of Sliding Spectral Windows for Parameter Estimation in Power System Disturbance Monitoring", *IEEE Trans. on Power Eng. Systems*, 2000.

[20] T. Painter and A. Spanias, "Perceptual Coding of Digital Audio", *Proc of the IEEE*, Vol. 88, No. 4, April 2000.

[21] P. Prandoni, M. Goodwin and M. Vetterli, "Optimal time segmentation for signal modeling and compression", *Proc. of Int. Conf. on Acoustic, Speech and Signal Processing (ICASSP)*, 1997.

[22] J.G. Proakis, *Digital Communications*, McGraw-Hill Companies, 1995.

[23] D.C. Rife and R.R. Boorstyn, "Single-Tone Parameter Estimation from Discrete-Time Observations", *IEEE Trans. on Information Theory*, vol. IT-20(5), 1974.

[24] P. Stoica and R. Moses, *Introduction to spectral analysis*, Prentice-Hall, 1997.

[25] S. Van Huffel, C. Decanniere, H. Chen and P. Van Hecke, "Algorithm for Time-Domain NMR Data Fitting Based on Total Least Squares", *Journal of Magnetic Resonance A*, Vol. 110, pp. 228-237, 1994.

[26] M. K. Varanasi and B. Aazhang, "Multistage Detection in Asynchronous CDMA Communications", *Trans. on Commun.*, Vol. 38, No. 4, pp. 508-519, April 1990.

[27] M. Vetterli and J. Kovacevic, *Wavelets and Subband Coding*, Prentice Hall, 1st Ed., 1995.

[28] T. Wigren and A. Nehorai, "Asymptotic Cramer-Rao Bounds for Estimation of the Parameters of Damped Sine Waves in Noise", *IEEE Trans. on Signal Processing*, Vol. 39, No. 4, pp. 1017-1020, April 1991.